Single cobalt sites in mesoporous N-doped carbon matrix for selective catalytic hydrogenation of nitroarenes

Sun, Xiaohui; Olivos-Suarez, Alma I.; Osadchii, Dmitrii; Romero, Maria Jose Valero; Kapteijn, Freek; Gascon, Jorge

DOI
10.1016/j.jcat.2017.10.030

Publication date
2018

Document Version
Final published version

Published in
Journal of Catalysis

Journal of Catalysis 357 (2018) 20–28

Contents lists available at ScienceDirect

Journal of Catalysis

journal homepage: www.elsevier.com/locate/jcat

Single cobalt sites in mesoporous N-doped carbon matrix for selective catalytic hydrogenation of nitroarenes

Xiaohui Sun [a], Alma I. Olivos-Suarez [b], Dmitrii Osadchii [a], Maria Jose Valero Romero [a], Freek Kapteijn [a], Jorge Gascon [a,b,*]

[a] Catalysis Engineering, Department of Chemical Engineering, Delft University of Technology, Van der Maasweg 9, 2629 HZ Delft, The Netherlands
[b] King Abdullah University of Science and Technology, KAUST Catalysis Center, Advanced Catalytic Materials, Thuwal 23955, Saudi Arabia

ARTICLE INFO

Article history:
Received 6 August 2017
Revised 13 October 2017
Accepted 30 October 2017
Available online 20 November 2017

Keywords:
Nitroarene
Hydrogenation
Co single atom
Chemoselectivity

ABSTRACT

A supported cobalt catalyst with atomically dispersed Co-N_x sites (3.5 wt% Co) in a mesoporous N-doped carbon matrix (named Co@mesoNC) is synthesized by hydrolysis of tetramethyl orthosilicate (TMOS) in a Zn/Co bimetallic zeolitic imidazolate framework (BIMZIF(Co,Zn)), followed by high-temperature pyrolysis and SiO_2 leaching. A combination of TEM, XRD XPS and X-ray absorption spectroscopy studies confirm the absence of cobalt nanoparticles and indicate that these highly dispersed cobalt species are present in the form of Co-N_x. The exclusive formation of Co-N_x sites in the carbon matrix is attributed to the presence of a large amount of Zn and N in the BIMZIF precursor together with the presence of SiO_2 in the pore space of this framework, extending the initial spatial distance between cobalt atoms and thereby impeding their agglomeration. The presence of SiO_2 during high-temperature pyrolysis is proven crucial to create mesoporosity and a high BET area and pore volume in the N-doped carbon support (1780 m^2 g^{-1}, 1.54 cm^3 g^{-1}). This heterogeneous Co@mesoNC catalyst displays high activity and selectivity (>99%) for the selective hydrogenation of nitrobenzene to aniline at mild conditions (0.5–3 MPa, 343–383 K). When more challenging substrates (functionalized nitroarenes) are hydrogenated, the catalyst Co@mesoNC displays an excellent chemoselectivity to the corresponding substituted anilines. The presence of mesoporosity improves mass transport of reactants and/or products and the accessibility of the active Co-N_x sites, and greatly reduces deactivation due to fouling.

1. Introduction

The reduction of nitroarenes to their substituted anilines is of great importance in organic synthesis and applied on large scale for the production of dyes, pharmaceuticals, pigments, and agrochemicals [1–4]. Hydrogen is attractive because it is one of the cleanest reductant [5–7]. Despite the development of a large number of molecular catalysts [8–12], in general these homogeneous catalysts suffer from difficulties in recycling and separation from products. Hence, heterogeneous catalysts containing supported metal nanoparticles (NPs) are more attractive [13–18]. Platinum-group metals have been proposed as alternative and are industrially used in the direct hydrogenation of nitroarenes [19–23]. Although they are highly efficient in the activation of nitro groups, these catalysts are also highly active for hydrogenolysis of carbon-halogen bonds (i.e. —F, —Cl, etc.) and hydrogenation of other reducible groups (i.e. C=O and C=C, etc.), which usually leads to poor chemoselectivity [24–28]. Thus, the exploration for advanced materials that catalyze the hydrogenation of nitroarenes maintaining high activities and without compromising chemoselectivity remains challenging.

Recently, tremendous efforts have led to the development of cheaper first-row transition-metal-based hydrogenation catalysts (i.e. Fe, Co, and Ni) [15,29–41]. Among these catalysts, N-doped carbon supported cobalt materials prepared by the carbonization of metal-organic-frameworks (MOFs) or a mixture of cobalt salts and organic complex exhibited good activity and chemoselectivity in the hydrogenation of nitroarenes [29–32,36,39–46]. There is a general agreement that cobalt plays an indispensable role in enhancing the hydrogenation activity of the catalysts. Yet, the heterogeneity of the cobalt species (i.e. accessible and inaccessible cobalt nanoparticles encapsulated by graphite shells, single cobalt atoms coordinated with nitrogen (Co-N_x), etc.) raises debate on what is the real active site in the hydrogenation process, and therefore greatly hinders the rational design and development of highly active and durable catalysts. Very recently, by one-step pyrolysis of

* Corresponding author at: King Abdullah University of Science and Technology, KAUST Catalysis Center, Advanced Catalytic Materials, Thuwal 23955, Saudi Arabia.
E-mail address: jorge.gascon@kaust.edu.sa (J. Gascon).

https://doi.org/10.1016/j.jcat.2017.10.030
0021-9517/

a cobalt-containing MOF (ZIF-67) under N_2 atmosphere followed by a subsequent acid treatment, we proved that the accessible cobalt nanoparticles in that system exhibit a high activity for this reaction [36]. Surprisingly, after acid leaching, the sample still shows outstanding hydrogenation activity. Although highly dispersed cobalt species (i.e. Co-N_x) are considered to exist in the acid-leached sample, the presence of those acid-resistant cobalt nanoparticles, fully encapsulated by multilayer graphitic carbon shells largely impedes further exploration of the structure-activity relation in this reaction. Hence, a rational design strategy that can preferentially produce active Co-N_x sites should be explored.

In view of the similar coordination of Co^{2+} and Zn^{2+} with 2-methylimidazole in ZIF-67 and ZIF-8 [47–49], a series of Zn/Co bimetallic zeolitic imidazolate framework (BIMZIF(Co,Zn)) have been recently reported, where the spatial distribution of Co and Zn in the framework is largely dependent on sequential addition of the metal precursors during synthesis [50–54]. Remarkably, when the precursors are added together, a homogeneous distribution of Zn and Co in the BIMZIF(Co,Zn) can be obtained. The presence of Zn^{2+} effectively separates Co atoms in the framework, and, to some extent, precludes their agglomeration into cobalt NPs during the high-temperature pyrolysis [52,53]. The carbon matrix generated using this strategy exhibits high surface area but normally microporosity [52,53], which can lead to significant internal mass transport limitations during the catalytic process, and therefore catalytic activity and stability can be severely inhibited [55,56].

Herein, we report a facile and easily scalable method to construct an atomically dispersed cobalt catalyst with a 3.5 wt% Co loading in a mesoporous N-doped carbon for chemoselective hydrogenation of nitroarenes to their substituted anilines under mild conditions. The catalyst is synthesized in several steps: (i) hydrolysis of tetramethyl orthosilicate (TMOS) in the pores of a BIMZIF(Co,Zn), followed by (ii) high-temperature pyrolysis and (iii) silica leaching. We demonstrate that the high Zn/Co molar ratio in the parent BIMZIF together with the SiO_2-protection strategy is crucial to impede the formation of cobalt nanoparticles and preferentially generate atomically dispersed Co-N_x sites. At the same time, the SiO_2-templated approach maintains a high specific surface area and generates mesoporosity in the N-doped carbon matrix. These Co-N_x sites in the mesoporous N-doped carbon matrix exhibit superior hydrogenation activity and chemoselectivity, and good catalytic stability. This strategy opens a path for the rational designing of highly active non-noble catalysts for hydrogenation reactions.

2. Experimental

2.1. Materials

2-Methylimidazole (MeIm, purity 99%), zinc nitrate hexahydrate ($Zn(NO_3)_2{\cdot}6H_2O$, >98%), cobalt nitrate hexahydrate ($Co(NO_3)_2{\cdot}6H_2O$, >99%), tetramethyl orthosilicate (TMOS $\geq$ 99%), and methanol (>99.8%) were purchased from Sigma-Aldrich Chemical Co. All the chemicals were used without further purification.

2.2. Catalyst synthesis

For the synthesis of BIMZIF(Co,Zn), a mixture of $Zn(NO_3)_2{\cdot}6H_2O$ and $Co(NO_3)_2{\cdot}6H_2O$ with Zn^{2+}/Co^{2+}molar ratio of 25 was dissolved in 200 mL methanol. A mixture of MeIm (6.489 g) in 200 mL methanol was rapidly poured into the above solution with vigorous stirring for 24 h at room temperature [52]. The total molar amount of (Co^{2+} + Zn^{2+}) was fixed to be 10 mmol. Afterwards, the products were collected by filtration, washed thoroughly with methanol, and dried overnight at 353 K under vacuum. For the synthesis of ZIF-8(Zn) and ZIF-67(Co), all the steps were the same except only $Zn(NO_3)_2{\cdot}6H_2O$ or $Co(NO_3)_2{\cdot}6H_2O$ and MeIm were used. Around 1 g ZIF materials can be produced from each batch.

1 g of the synthesized BIMZIF(Co,Zn) was suspended in 5 mL TMOS in an autoclave, and further transferred into a rotation oven and heated up to 333 K overnight. After the oven was cooled down to room temperature, the mixture was carefully washed with 0.5 mL ethanol by filtration. Then the obtained BIMZIF@TMOS material was placed in a cotton thimble of 22 mm diameter inside a glass tube of 25 mm diameter. The glass tube was fitted to a round bottom flask containing 500 ml of water. A needle to bubble 10 ml min^{-1} of N_2 flux into water was also fitted. The temperature was raised to 323 K to create a wet N_2 stream to hydrolyze the TMOS molecules for 24 h, after which the sample was collected and dried in an oven at 333 K overnight. The obtained sample was denoted as BIMZIF@SiO_2, with the yield of 1.2 g.

Co@NC-SiO_2 was prepared by pyrolysis of 1 g BIMZIF@SiO_2 at 1173 K for 4 h under N_2 at a ramp of 2 K min^{-1}, with the yield of 0.44 g. The obtained Co@NC-SiO_2 was further leached in 1 M NaOH solution for 24 h to remove the SiO_2 template, followed by washing with deionized water until the pH reached neutral, and dried at 323 K overnight under vacuum to afford Co@mesoNC sample, with the yield of 0.23 g.

For comparison, Co@NC and NC were prepared by pyrolysis of 1 g BIMZIF(Co,Zn) and ZIF-8 at 1173 K for 4 h under N_2 at a ramp of 2 K min^{-1}, respectively. The pyrolyzed ZIF-67 sample was obtained by pyrolysis of ZIF-67 at 1073 K for 8 h under N_2 using a temperature ramp of 2 K min^{-1}.

2.3. Characterization

X-ray diffraction (XRD) patterns were recorded on a Bruker D8 Advance X-ray diffractometer equipped with a Co-$K\alpha$ radiation (λ = 0.179026 nm). Transmission electron microscopy (TEM) and high-resolution TEM (HR-TEM) were performed by using a Talos F200X microscope (FEI, Hillsboro, OR, USA) at an acceleration voltage of 200 kV. Raman spectra were obtained with a commercial Renishaw in Via Reflex confocal microscope using a 532 nm laser. Measurements were carried out in samples without any pretreatment at ambient conditions. The N_2 adsorption-desorption measurements were performed by using a Micromeritics Tristar 3020 apparatus at 77 K [57]. Prior to measurement, samples were degassed under vacuum at 383 K overnight. The Co and N contents in the samples were measured by atomic adsorption spectroscopy (AAS) (Analyst 200, Perkin Elmer, USA) and elemental analysis (Vario EL, Elementar, Germany), respectively. XPS measurements were performed on a *K*-alpha Thermo Fisher Scientific spectrometer using monochromatic Al-*K* radiation at ambient temperature and chamber pressure of about 10^{-8} mbar. All the spectra measured were corrected by setting the reference binding energy of carbon (*1s*) at 284.8 eV.

X-ray absorption experiments were performed at DUBBLE beam line BM26A in ESRF, Grenoble. The materials were studied using Co K-edge. Energy calibration was achieved using metal foil as reference and the first peak in the first derivative of the metal foil XAS spectrum was calibrated to 7709 eV [58]. Calibration and data alignment was performed using Athena and reference compounds values were obtained from Hephaestus. After averaging, the spectra of the studied samples were normalized to a total absorption of unity and processed using the Athena data normalization and analysis package [59]. For normalization, the spline *r*-background parameter was set to 1.0. The background subtraction was carried using a pre-edge range of −200 to −30 eV and a post-edge linear range of 50–985 eV. A spline range of k = 0 to k = 14.8 A^{-1} and

k-weight of 3 was used to isolate the EXAFS (chi)function. The Co *K*-edge EXAFS spectra were Fourier transformed over a *k*-range of $k = 3$ to $k = 11$ Å^{-1}. Fitting of Co K-edge EXAFS spectra was carried out by Artemis software [60]. The spectra of the different samples were fitted in *R*-space with a *R* range of 1– 4.5 Å, and the fittings were done with a *k*-weight of 3. The Fourier transform and inverse Fourier transform was carried with a Δk of 1 and ΔR of 0. From the references fits we obtain the amplitude factor (S_0^2) equal to 0.77 ± 0.03 for cobalt foil and to 0.73 ± 0.13 for CoO. In further fittings of the experimental samples $S_0^2 = 0.73$ was used.

2.4. Catalyst performance

In a typical experiment, hydrogenation reactions are carried out in a batch mode, for which the autoclave is filled with nitrobenzene (1 mmol), an internal standard (dodecane, 0.65 mmol), the Co@mesoNC catalyst with a substrate to cobalt molar ratio of 150, and ethanol (5 ml) as solvent. Before starting the reaction, the autoclaves are purged 3 times with He to remove air, and pressurized to 3 MPa H_2, followed by heating to 383 K. After a fixed reaction time, the autoclaves are cooled down to room temperature and the hydrogen pressure is carefully released. The stirring speed is kept at 800 rpm to avoid mass transfer limitations. For recycling studies, the reaction was performed under the same conditions as mentioned above except using the recovered catalyst. The used catalyst was filtered and washed thoroughly with ethanol, dried under vacuum at 313 K overnight and then used for the next run without any reactivation or purification. Conversions of all substrates were determined by gas chromatography (GC) analysis.

3. Results and discussion

3.1. Preparation and characterization of the Co@mesoNC catalyst

Fig. 1 illustrates the preparation process for the Co@mesoNC catalyst. In the first step, the BIMZIF(Co,Zn) was synthesized by reacting Co^{2+} and Zn^{2+} ions with 2-methylimidazole (MeIm) in methanol. Then tetramethyl orthosilicate (TMOS) was introduced into the pores of BIMZIF followed by hydrolysis to obtain BIMZIF@SiO_2 material. Finally, the BIMZIF@SiO_2 sample was pyrolyzed at 1173 K, and the SiO_2 template was subsequently leached with a NaOH solution to generate the Co@mesoNC catalyst (see Experiment Section for the details).

The powder X-ray diffraction (XRD) pattern (Fig. S1) of the bimetallic ZIF matches well with ZIF-8 (Zn), confirming the successful synthesis [36,48]. High-angle annular dark-field scanning transmission electron microscopy (HAADF-STEM) (Fig. S2a) and energy-dispersive X-ray spectroscopy (EDX) (Fig. S2b–e) images of the prepared BIMZIF crystals with a size of 30–50 nm clearly exhibit a typical rhombic dodecahedral shape with homogeneously dispersed cobalt, zinc, carbon and nitrogen throughout the crystals. The tracking of each synthetic step for Co@mesoNC by TEM combined with elemental mapping analysis confirms the uniform distribution of Si and Co in both BIMZIF@SiO_2 (Fig. S3a–c) and Co@NC-SiO_2 materials (Fig. S3d–f), and highlights the absence of cobalt nanoparticles in Co@NC-SiO_2 (Fig. S4). After removal of the SiO_2 template, the absence of cobalt nanoparticles in the Co@mesoNC catalyst is further confirmed in Fig. 2a,b, while uniformly dispersed Co and N EDX-signals can be clearly detected throughout the catalyst (Fig. 2c,d). The atomic adsorption spectroscopy (AAS) and elemental analysis indicate that the Co@mesoNC catalyst has 3.5 wt% Co and 15.0 wt% N. At the same time, 2.8 wt% Zn and 1.6 wt% Si are also detected in Co@mesoNC, indicative of some residual Zn and Si in the sample even after high-temperature pyrolysis and NaOH washing. The high-resolution TEM (HR-TEM) image of Co@mesoNC in the insert of Fig. 2a clearly demonstrates the presence of a layered graphitic carbon structure with a typical interplanar distance of 0.34 nm. The absence of cobalt nanoparticles is further supported by powder XRD analysis (Fig. 3a). No cobalt (oxide) reflections can be identified, and only two diffractions at $2\theta = 30°$ and 50.5° are observed, attributed to the (0 0 2) and (1 0 0) planes of the graphitic carbon, respectively [61]. The graphitization degree of the carbon matrix in the Co@mesoNC sample was further analyzed by Raman spectroscopy (Fig. S5). The characteristic D and G bands of carbon at 1350 cm^{-1} and 1580 cm^{-1} are clearly observed, correlated to graphitic disordered or defective carbon and sp^2-bonded graphitic carbon sheets, respectively [62,63]. The BET area (S_{BET}) and pore volume (V_{pore}) of the BIMZIF and Co@mesoNC were determined by N_2 adsorption-desorption isotherms, as shown in Fig. 3b and Table S1. BIMZIF, with a high S_{BET} of 1780^2 g^{-1} and V_{pore} of 1.44 cm^3 g^{-1}, displays a steep N_2 uptake at low relative pressures, typically associated with microporosity [50]. A hysteresis loop above $P/P_0 \approx 0.8$ is also observed for BIMZIF, suggesting the presence of intergranular mesoporosity between the nanocrystals. After high-temperature pyrolysis and SiO_2 leaching, Co@mesoNC exhibits a S_{BET} of 1230^2 g^{-1} and V_{pore} of 1.54 cm^3 g^{-1}. At the same time, the N_2 adsorption-desorption isotherms of Co@mesoNC change to type IV with type H_3 hysteresis that closes at $P/P_0 \approx 0.4$, suggesting the presence of mesoporous structure inside the nanoparticles [64,65].

The Co@mesoNC catalyst was further characterized by means of X-ray photoelectron spectroscopy (XPS). As shown in Fig. 4a, N1s signals of Co@mesoNC can be described by the combination of four types of nitrogen species with binding energy around 398.5 eV, 399.8 eV, 400.8 eV, and 402.3 eV, which can be attributed to pyridinic-N (53.4 at.%), pyrrolic-N (25.5 at.%), quaternary-N (17.0 at.%) and oxidized-N (4.1 at.%), respectively [66,67]. We speculate

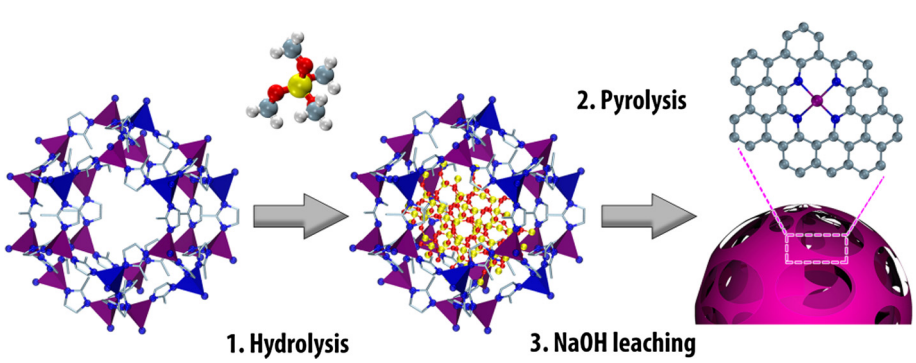

Fig. 1. Schematic illustration of the synthesis of the Co@mesoNC catalyst. (1) Impregnation and hydrolysis of TMOS molecules in the porosity of BIMZIF. (2) Pyrolysis of the mixture of BIMZIF@SiO_2 in N_2 to decompose BIMZIF and form Co@NC-SiO_2. (3) NaOH leaching to remove SiO_2 to generate the Co@mesoNC catalyst.

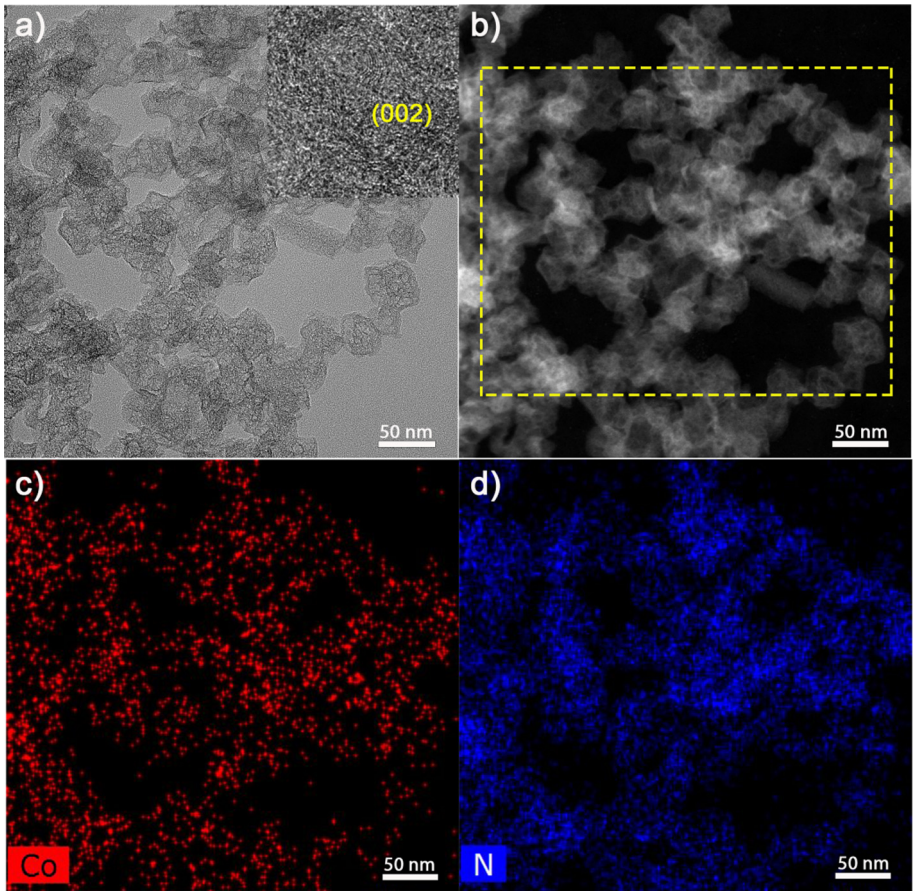

Fig. 2. Bright field (a) and dark field (b) TEM image of Co@mesoNC catalyst; element mapping image of Co (c) and N (d) for Co@mesoNC catalyst.

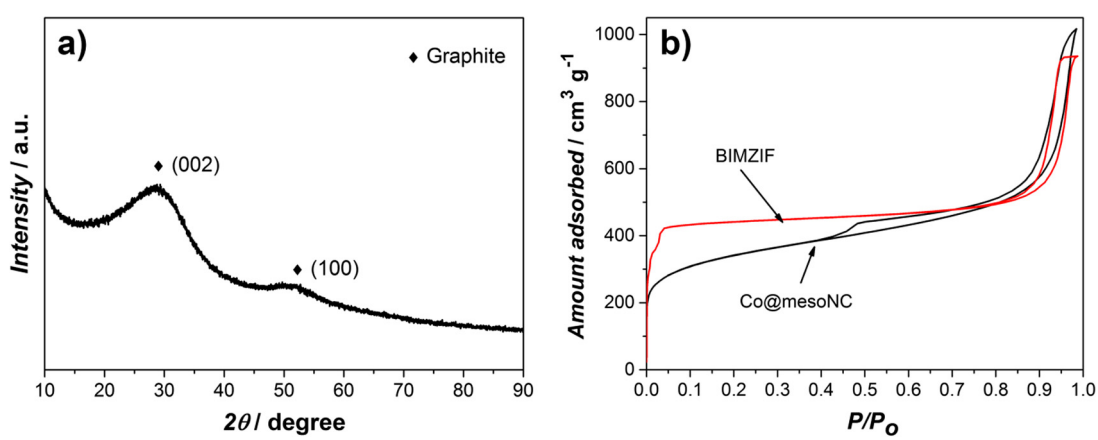

Fig. 3. (a) XRD pattern of Co@mesoNC catalyst; (b) N_2-adsorption-desorption isotherms of BIMZIF and Co@mesoNC materials.

that, upon pyrolysis, N atoms in the pentagonal ring of the original imidazole units are mostly converted into pyridinic-, pyrrolic-, and quaternary-N species. The Co*2p* XPS spectrum of Co@mesoNC in Fig. 4b highlights the absence of metallic Co (usually at 778.5 eV), while the peak at 780.5 eV can be ascribed to Co-N_x species [53,61,68].

Co K-edge X-ray absorption spectroscopy (XAS) measurements were carried out to further explore the local environment of cobalt in the Co@mesoNC sample. As shown in the X-ray absorption near-edge structure (XANES) spectrum (Fig. 4c), a well-developed peak at 7709 eV in the pre-edge region can be observed in the BIMZIF sample, arising from the electronic transition from the core *1s* to the unoccupied *3d* orbitals. This intense pre-edge peak clearly reveals that the local symmetry around cobalt ions is not centrosymmetric, confirming the tetrahedral symmetry around central cobalt atoms [69]. The edge energy (E_0), located at 7717 eV, suggest the presence of divalent Co in the original framework. After pyrolysis and SiO_2 removal, the edge for Co@mesoNC is situated at 7720 eV and is higher in energy to that of metallic Co in the pyrolyzed ZIF-67 at 7709 eV, indicating that no metallic cobalt phase is present in Co@mesoNC. The lower intensity of the pre-edge feature in Co@mesoNC compared to that of the original BIMZIF suggests

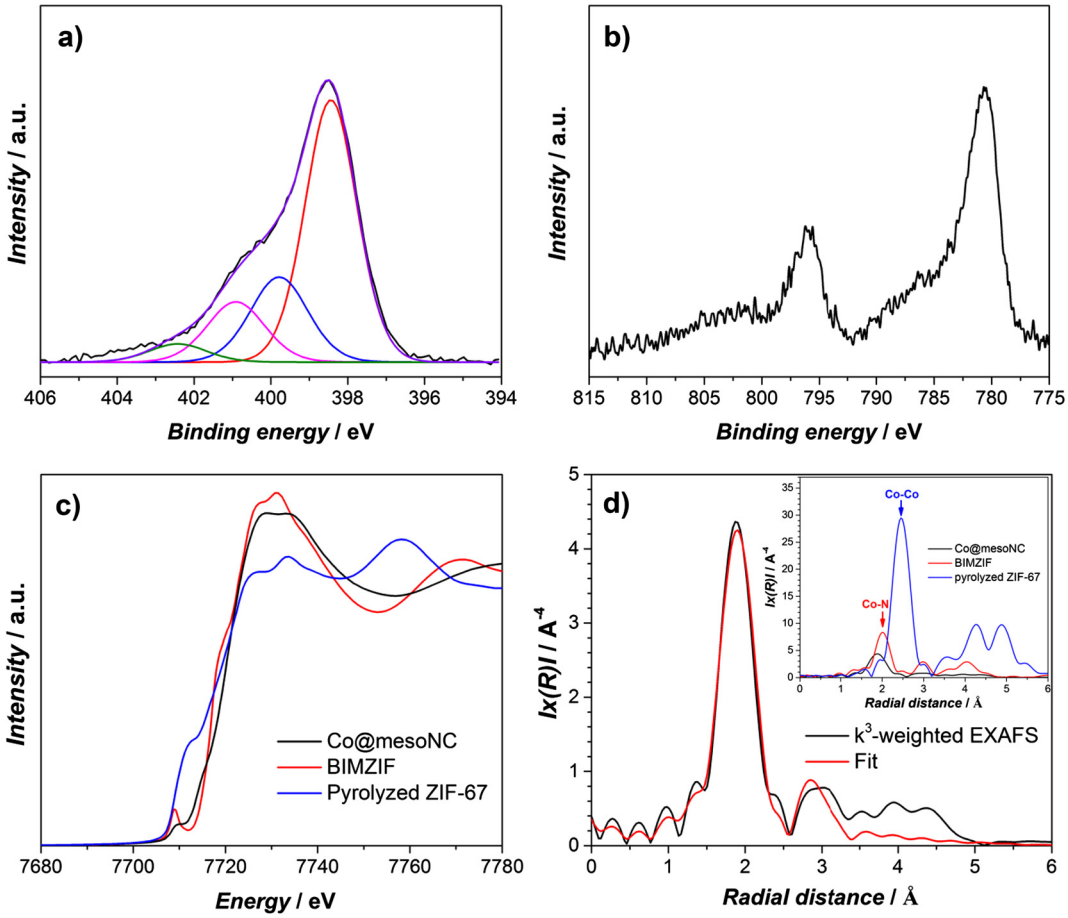

Fig. 4. N*1s* (a) and Co*2p* (b) XPS regions of Co@mesoNC catalyst; (c) Co *K*-edge XANES spectra; and (d) Fitting of phase corrected k^3-weighted $\chi(k)$-function EXAFS spectra of Co@mesoNC catalyst, together with the phase corrected Co@mesoNC, BIMZIF and pyrolyzed ZIF-67 in the inset.

that the tetrahedral coordination environment of cobalt in the framework changed during the high-temperature pyrolysis process. Similar shape, intensity and location of the pre-edge feature has been observed in case of quadrupole *1s* → *3d* transition in distorted octahedral coordination environment [70–72]. The similar location of the white line (with a threshold energy of 7731 eV) and the marked differences of the continuous resonance shape between both samples (BIMZIF and Co@mesoNC) also confirms a drastic change in the local geometry around cobalt [69].

Further local structural information can be obtained from extended X-ray absorption fine structure (EXAFS, Fig. 4d). The fittings of the R-space curve for BIMZIF yields a first Co-N coordination sphere at 1.99 Å bond distance (inset of Figs. 4d and S7c,d) [53,69]. After pyrolysis, the first coordination sphere around Co shifts to a lower bond distance (1.89 Å), demonstrating that the coordination of Co varies slightly. Importantly, in the fittings of the EXAFS signal for Co@mesoNC it was not possible to include any Co-Co scattering paths with reasonable parameters (Fig. S6 and Table S2). In contrast, the metallic Co nanoparticles in the pyrolyzed ZIF-67 (Fig. S7e,f and Table S2) clearly show exclusively the Co-Co path that can be fitted with Co-Co bond distances of 2.49 Å. These marked differences further confirm that Co is atomically dispersed in the Co@mesoNC sample.

To clarify the role of SiO_2 during the synthesis, we prepared a sample, denoted as Co@NC, by direct pyrolysis of BIMZIF. In the absence of SiO_2 during pyrolysis, both cobalt nanoparticles and highly dispersed Co-N_x species can be observed in the TEM image of this sample (Fig. S8a–d), although it exhibits a comparable graphitization degree as the Co@mesoNC sample, as concluded from a similar I_D/I_G ratio in the Raman spectra (Fig. S5). In addition, N_2 adsorption-desorption isotherms indicate that Co@NC exhibits a typical microporous structure with some intergranular mesoporosity, as concluded from the presence of hysteresis loop above $P/P_0 \approx 0.8$ (Fig. S9). The Brunauer-Emmett-Teller area (S_{BET}) and pore volume (V_{pore}) of Co@NC are 680 m^2 g^{-1} and 0.98 m^3 g^{-1}, much lower than that of Co@mesoNC (1230 m^2 g^{-1} and 1.54 m^3 g^{-1}) (Table S1), attributed to the collapse of the well-defined microporous structure of BIMZIF during the pyrolysis process [36,73].

The preferred formation of Co-N_x sites and the absence of cobalt nanoparticles in the Co@mesoNC catalyst can be attributed to the following: (i) When a large amount of Zn is present in the original BIMZIF material, the spatial distance between two Co atoms can be finely controlled by Zn atoms acting as a spacer, thereby precluding the agglomeration of cobalt atoms to nanoparticles during the high-temperature pyrolysis; (ii) During the pyrolysis process, Zn evaporate [74], and free N-coordination sites can be generated in the carbon matrix, which help stabilize the Co atoms [52,53] and (iii) The presence of SiO_2 nanoparticles in the well-developed porosity of BIMZIF further mitigates the sintering of Co atoms under high-temperature pyrolysis condition [75]. Thus, the SiO_2-templated strategy in this work impedes the formation of cobalt nanoparticles, creates mesoporosity and maintains a high specific surface area in the N-doped carbon matrix.

3.2. Catalytic hydrogenation of nitrobenzene to aniline over the Co@mesoNC catalyst

Direct hydrogenation of nitrobenzene with H_2 requires an efficient catalyst to simultaneously promote the activation of hydro-

Table 1
Results of the catalytic hydrogenation of nitrobenzene over the prepared catalysts.[a]

Entry	Sample	T (K)	P (MPa)	X_{Nitro} (%)	$S_{Aniline}$ (%)	TOF [b]	Catalyst productivity ($mmol_{NB}$ h^{-1} mg_{Co}^{-1})[c]
1	No catalyst	383	3	–	–	–	–
2[d]	Co@mesoNC	383	3	–	–	–	–
3	BIMZIF	383	3	–	–	–	–
4[e]	NC	383	3	–	–	–	–
5	Co@mesoNC	383	3	55	>99	42	0.72
6	Co@mesoNC	383	0.5	14	>99	11	0.18
7	Co@mesoNC	383	1	25	>99	19	0.32
8	Co@mesoNC	383	2	43	>99	33	0.55
9	Co@mesoNC	343	3	12	>99	9	0.15
10	Co@mesoNC	363	3	27	>99	21	0.34

[a] Reaction conditions: 1 mmol nitrobenzene, 11 mg catalyst, substrate to cobalt molar ratio of 150, 0.65 mmol dodecane as internal standard, 5 mL ethanol, 383 K, 3 MPa H_2, 2 h.
[b] *TOF* = moles of converted substrate per mole of Co atoms per hour. Considering that only single cobalt sites are present in Co@mesoNC, all cobalt atoms participate in the reaction.
[c] Calculated by moles of nitrobenzene consumed divided by total weight of cobalt per hour.
[d] Reaction was performed in He atmosphere.
[e] Prepared by pyrolysis of ZIF-8 crystals under N_2 flow.

gen and nitro groups in the substrates. In order to clearly understand the catalytic activity of the Co@mesoNC catalyst in this process, a series of control experiments were firstly performed. As shown in Table 1, hydrogenation of nitrobenzene to aniline did not proceed in the absence of catalyst (Entry 1, Table 1) or H_2 (Entry 2, Table 1). Similarly, no aniline was detected over the original BIMZIF (Entry 3, Table 1) and the 'NC' sample prepared by pyrolysis of ZIF-8 (Entry 4, Table 1) under the same conditions. However, the Co@mesoNC sample efficiently catalyzed the hydrogenation of nitrobenzene to aniline without any other detectable products (Entry 5, Table 1). These results reveal that the highly dispersed Co-N_x species generated during high temperature pyrolysis are the active sites for the chemoselective hydrogenation of nitro groups. In addition, the hydrogenation activity of the Co@mesoNC catalyst is dependent on H_2 pressure (Entries 5–8, Table 1) and reaction temperature (Entry 5, Entries 9–10, Table 1). Obviously, a higher H_2 pressure and a high reaction temperature promote the hydrogenation; hence in all subsequent experiments the reaction conditions were fixed at 3 MPa H_2 and 383 K. Importantly, the kinetic profile of the reaction in Fig. 5a indicates that nitrobenzene could be converted smoothly into aniline with initially a nearly zero order in concentration, and no intermediates could be detected by gas chromatography during the entire reaction process. Interestingly, the catalytic activity of Co@mesoNC is superior to the behavior of other recently reported supported cobalt catalysts (Table S3), such as Co@N-doped carbon [29], CoO_x@NCNTs [30], Co-SiCN [31], and Co-Co_3O_4/NGr@C [42].

The stability and reusability of the Co@mesoNC catalyst was also investigated. As presented in Fig. 5b, under the studied conditions, the Co@mesoNC catalyst exhibits a nitrobenzene conversion of 73% after 3 h, and can be reused at least four times with a nitrobenzene conversion still above 51% after the fourth run. The TEM image of the spent Co@mesoNC after the fourth run shows that the Co atoms in the N-doped carbon matrix are still well dispersed and no cobalt nanoparticles can be detected (Fig. S10), excluding the agglomeration of cobalt as a major cause of deactivation during hydrogenation. The structure of the spent Co@mesoNC catalyst is still well preserved as revealed by the Raman spectrum in Fig. S11 and XPS analysis in Fig. S12, suggesting that the deactivation cannot be attributed to any modification in the carbon structure during the hydrogenation process. ICP analysis of the reaction mixture indicates a small amount of cobalt (~3 wt% of the total cobalt content) in solution after each run (Table S4). At the same time, after each run, a slight increase of catalyst mass (~2%) was observed even after a thorough washing with ethanol and vacuum drying, indicative of some residual deposit in the pores of the catalysts, which cannot be easily removed. Hence, the deactivation of Co@mesoNC catalyst is ascribed mainly to foul-

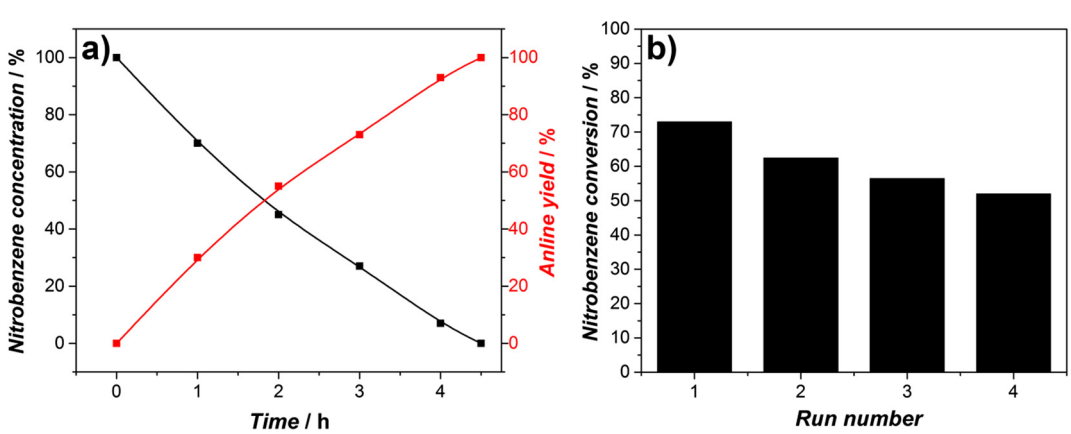

Fig. 5. (a) Kinetic data of hydrogenation of nitrobenzene with Co@mesoNC catalyst. The plot is based on the results of different reactions stopped at different times. (b) Recycling experiments of hydrogenation of nitrobenzene with Co@mesoNC catalyst. Reaction conditions: 1 mmol nitrobenzene, 11 mg catalyst, substrate to cobalt molar ratio of 150, 0.65 mmol dodecane as internal standard, 5 mL ethanol, 383 K, 3 MPa H_2, 3 h for recycling experiments. Aniline selectivity > 99%.

Table 2
Results of the chemoselective hydrogenation of substituted nitroarenes over Co@mesoNC.[a]

Entry	Substrate	Product	S (%)[b]	Catalyst productivity ($mmol_{Nitro}$ h^{-1} mg_{Co}^{-1})[c]
1	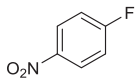	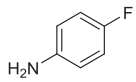	>98	0.70
2	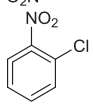	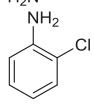	>99	0.79
3	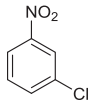	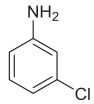	>99	0.79
4	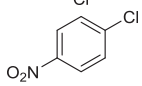	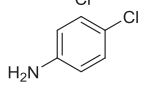	>98	0.75
5	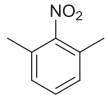	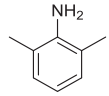	>99	0.40
6	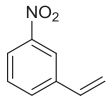	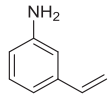	>97	0.46
7	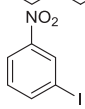	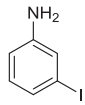	>97	0.22
8	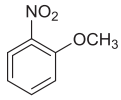	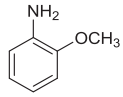	>98	0.53
9[d]	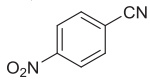	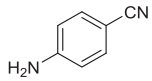	>93	0.51
10[d]	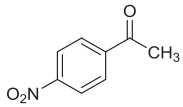	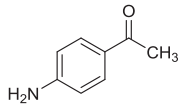	>96	0.48

[a] Reaction conditions: 1 mmol nitrobenzene, 11 mg catalyst, substrate to cobalt molar ratio of 150, 0.65 mmol dodecane as internal standard, 5 mL ethanol, 383 K, 3 MPa H_2, 2 h.
[b] Selectivity to the substituted anilines.
[c] Calculated by moles of nitroarenes consumed divided by total mass of cobalt per hour.
[d] Reaction time 3 h.

ing by unidentified deposits during reaction, although some minute loss of cobalt cannot be excluded. This fouling is stronger for the microporous Co@NC sample prepared by direct pyrolysis of BIMZIF(Co,Zn). After an initial nitrobenzene conversion of only 34%, this decreases sharply to 6% after 4 consecutive runs (Fig. S13) under similar reaction conditions. The inferior hydrogenation performance of Co@NC further demonstrates the high activity of these highly dispersed Co-N_x sites in the mesoporous carbon matrix, which contributes to the accessibility of the active Co-N_x sites and improved mass transport of substrate molecules during the hydrogenation process.

3.3. Co@mesoNC catalyzed hydrogenation of nitroarenes to substituted anilines

To explore the general applicability of Co@mesoNC, a variety of substituted nitroarenes containing electron-donating and electron-withdrawing groups at different positions were investigated under the standard test conditions. As shown in Table 2, the Co@mesoNC catalyst exhibits a high activity for the hydrogenation of industrially relevant nitroarenes such as fluoro- and chloronitrobenzenes toward their corresponding anilines in high selectivities (Table 2, entries 1–4). Even a sterically hindered nitroarene was hydrogenated to the substituted aniline with outstanding activity and chemoselectivity (Table 2, entry 5). As it is well known, the most-challenging substrates are those that bear other easily reducible groups (Table 2, entries 6–10). Like other N-doped carbon supported metal catalysts prepared using high-temperature pyrolysis strategy [29–32,36–39,42], the Co@mesoNC catalyst is able to chemoselectively reduce nitro groups in the presence of C=C bonds with high activity (Table 2, entry 6 and Table S5), which is hardly achieved by Pt-group and Ni catalysts [39,42]. Furthermore, substrates containing sensitive groups, such as —I, —OCH_3, and —$COCH_3$, can be as well smoothly and chemoselectively hydrogenated into the corresponding anilines without dehalogenation and/or competitive hydrogenation on these substituted moieties (Table 2, entries 7–10). All these results demonstrate again that the atomically dispersed Co-N_x sites in the mesoporous N-doped carbon matrix displays excellent catalytic activity and chemoselectivity for hydrogenation of nitroarenes using molecular hydrogen.

4. Conclusions

In this work, a strategy is presented to synthesize a supported cobalt catalyst with atomically dispersed Co-N_x sites (3.5 wt% Co) in a mesoporous N-doped carbon matrix. The synthesis process consists of hydrolysis of TMOS molecules in BIMZIF(Co,Zn), high-temperature pyrolysis and removal of the SiO_2 template. The preferential formation and high stability of these Co-N_x sites in the carbon support are attributed to the presence of a large amount of Zn and N in the structure of the BIMZIF precursor and the presence of SiO_2 in the porosity of BIMZIF, which, to a large extent, effectively separates cobalt atoms, thereby impeding their agglomeration to nanoparticles. The SiO_2-templated approach is proven essential to generate mesoporosity in the N-doped carbon support and to maintain a high specific surface area in the carbon support during high-temperature pyrolysis as well. These Co-N_x sites in the mesoporous N-doped carbon matrix exhibit an outstanding activity and selectivity for the chemoselective hydrogenation of nitroarenes for a wide range of substrates under mild reaction conditions. The mesoporosity of this catalyst probably guaranteed a good mass transport of reactants and/or products and the accessibility of the active Co-N_x sites, thereby also reducing the deactivation of the catalyst by fouling.

Acknowledgments

We thank for the support from the Dutch-Belgian program for access to the BM26A in ESRF, Grenoble. We thank A. Dikhtiarenko for help in the design of the graphical abstract. Xiaohui Sun acknowledges financial support from China Scholarship Council (CSC).

Appendix A. Supplementary material

Supplementary data associated with this article can be found, in the online version, at https://doi.org/10.1016/j.jcat.2017.10.030.

References

[1] R.S. Downing, P.J. Kunkeler, H. van Bekkum, Catalytic amination reactions catalytic syntheses of aromatic amines, Catal. Today 37 (1997) 121–136.
[2] N. Ono, The Nitro Group in Organic Synthesis, Wiley-VCH, New York, 2001.
[3] H.-U. Blaser, H. Steiner, M. Studer, Selective catalytic hydrogenation of functionalized nitroarenes: an update, ChemCatChem 1 (2009) 210–221.
[4] H.-U. Blaser, C. Malan, B. Pugin, F. Spindler, H. Steiner, M. Studer, Selective hydrogenation for fine chemicals: recent trends and new developments, Adv. Synth. Catal. 345 (2003) 103–151.
[5] P.N. Rylander, Catalytic Hydrogenation in Organic Syntheses: Paul Rylander, Academic Press Incorporated, 1979.
[6] J.G. de Vries, C.J. Elsevier, The handbook of homogeneous hydrogenation, Wiley-VCH, 2007.
[7] P.G. Andersson, I.J. Munslow, Modern Reduction Methods, Wiley, 2008.
[8] F. L'Eplattenier, P. Matthys, F. Calderazzo, Homogeneous ruthenium-catalyzed reduction of nitrobenzene, Inorg. Chem. 9 (1970) 342–345.
[9] A. Corma, C. González-Arellano, M. Iglesias, F. Sánchez, Gold complexes as catalysts: chemoselective hydrogenation of nitroarenes, Appl. Catal. A 356 (2009) 99–102.
[10] K. Junge, K. Schroder, M. Beller, Homogeneous catalysis using iron complexes: recent developments in selective reductions, Chem. Commun. 47 (2011) 4849–4859.
[11] R.J. Rahaim, R.E. Maleczka, Pd-catalyzed silicon hydride reductions of aromatic and aliphatic nitro groups, Org. Lett. 7 (2005) 5087–5090.
[12] P.M. Reis, B. Royo, Chemoselective hydrogenation of nitroarenes and deoxygenation of pyridine N-oxides with H2 catalyzed by MoO2Cl2, Tetrahedron Lett. 50 (2009) 949–952.
[13] S. Nishimura, Handbook of Heterogeneous Catalytic Hydrogenation for Organic Synthesis, Wiley, 2001.
[14] R.A. Sheldon, H. Bekkum, Fine Chemicals Through Heterogenous Catalysis, Wiley-VCH, 2001.
[15] R.V. Jagadeesh, A.-E. Surkus, H. Junge, M.-M. Pohl, J. Radnik, J. Rabeah, H. Huan, V. Schünemann, A. Brückner, M. Beller, Nanoscale Fe2O3-based catalysts for selective hydrogenation of nitroarenes to anilines, Science 342 (2013) 1073–1076.
[16] A. Corma, P. Serna, Chemoselective hydrogenation of nitro compounds with supported gold catalysts, Science 313 (2006) 332–334.
[17] Y. Chen, C. Wang, H. Liu, J. Qiu, X. Bao, Ag/SiO2: a novel catalyst with high activity and selectivity for hydrogenation of chloronitrobenzenes, Chem. Commun. (2005) 5298–5300.
[18] A. Onopchenko, E.T. Sabourin, C.M. Selwitz, Selective catalytic hydrogenation of aromatic nitro groups in the presence of acetylenes. Synthesis of (3-aminophenyl)acetylene via hydrogenation of dimethylcarbinol substituted (3-nitrophenyl)acetylene over heterogeneous metallic ruthenium catalyst, J. Organ. Chem. 44 (1979) 1233–1236.
[19] G. Vilé, N. Almora-Barrios, N. López, J. Pérez-Ramírez, Structure and reactivity of supported hybrid platinum nanoparticles for the flow hydrogenation of functionalized nitroaromatics, ACS Catal. 5 (2015) 3767–3778.
[20] A. Yarulin, C. Berguerand, I. Yuranov, F. Cárdenas-Lizana, I. Prokopyeva, L. Kiwi-Minsker, Pt–Zn nanoparticles supported on porous polymeric matrix for selective 3-nitrostyrene hydrogenation, J. Catal. 321 (2015) 7–12.
[21] M. Carrus, M. Fantauzzi, F. Riboni, M. Makosch, A. Rossi, E. Selli, J.A. van Bokhoven, Increased conversion and selectivity of 4-nitrostyrene hydrogenation to 4-aminostyrene on Pt nanoparticles supported on titanium-tungsten mixed oxides, Appl. Catal. A 519 (2016) 130–138.
[22] J. Gu, Z. Zhang, P. Hu, L. Ding, N. Xue, L. Peng, X. Guo, M. Lin, W. Ding, Platinum nanoparticles encapsulated in MFI zeolite crystals by a two-step dry gel conversion method as a highly selective hydrogenation catalyst, ACS Catal. 5 (2015) 6893–6901.
[23] S. Zhang, C.-R. Chang, Z.-Q. Huang, J. Li, Z. Wu, Y. Ma, Z. Zhang, Y. Wang, Y. Qu, High catalytic activity and chemoselectivity of sub-nanometric Pd clusters on porous nanorods of CeO2 for hydrogenation of nitroarenes, J. Am. Chem. Soc. 138 (2016) 2629–2637.
[24] A. Corma, P. Serna, P. Concepción, J.J. Calvino, Transforming nonselective into chemoselective metal catalysts for the hydrogenation of substituted nitroaromatics, J. Am. Chem. Soc. 130 (2008) 8748–8753.
[25] G.C. Bond, Supported metal catalysts: some unsolved problems, Chem. Soc. Rev. 20 (1991) 441–475.
[26] B. Coq, A. Tijani, R. Dutartre, F. Figuéras, Influence of support and metallic precursor on the hydrogenation of p-chloronitrobenzene over supported platinum catalysts, J. Mol. Catal. 79 (1993) 253–264.
[27] X. Han, R. Zhou, G. Lai, X. Zheng, Influence of support and transition metal (Cr, Mn, Fe Co, Ni and Cu) on the hydrogenation of p-chloronitrobenzene over supported platinum catalysts, Catal. Today 93–95 (2004) 433–437.
[28] S. Kataoka, Y. Takeuchi, A. Harada, T. Takagi, Y. Takenaka, N. Fukaya, H. Yasuda, T. Ohmori, A. Endo, Microreactor containing platinum nanoparticles for nitrobenzene hydrogenation, Appl. Catal. A 427–428 (2012) 119–124.
[29] D. Formenti, F. Ferretti, C. Topf, A.-E. Surkus, M.-M. Pohl, J. Radnik, M. Schneider, K. Junge, M. Beller, F. Ragaini, Co-based heterogeneous catalysts from well-defined α-diimine complexes: discussing the role of nitrogen, J. Catal. 351 (2017) 79–89.
[30] Z. Wei, J. Wang, S. Mao, D. Su, H. Jin, Y. Wang, F. Xu, H. Li, Y. Wang, In Situ-Generated Co0-Co3O4/N-doped carbon nanotubes hybrids as efficient and chemoselective catalysts for hydrogenation of nitroarenes, ACS Catalysis 5 (2015) 4783–4789.
[31] T. Schwob, R. Kempe, A reusable Co catalyst for the selective hydrogenation of functionalized nitroarenes and the direct synthesis of imines and benzimidazoles from nitroarenes and aldehydes, Angew. Chem. Int. Ed. 55 (2016) 15175–15179.
[32] T. Cheng, H. Yu, F. Peng, H. Wang, B. Zhang, D. Su, Identifying active sites of CoNC/CNT from pyrolysis of molecularly defined complexes for oxidative esterification and hydrogenation reactions, Catal. Sci. Technol. 6 (2016) 1007–1015.
[33] B. Chen, F. Li, Z. Huang, G. Yuan, Recyclable and selective nitroarene hydrogenation catalysts based on carbon-coated cobalt oxide nanoparticles, ChemCatChem 8 (2016) 1132–1138.
[34] G. Hahn, J.-K. Ewert, C. Denner, D. Tilgner, R. Kempe, A reusable mesoporous nickel nanocomposite catalyst for the selective hydrogenation of nitroarenes in the presence of sensitive functional groups, ChemCatChem 8 (2016) 2461–2465.
[35] S. Pisiewicz, D. Formenti, A.-E. Surkus, M.-M. Pohl, J. Radnik, K. Junge, C. Topf, S. Bachmann, M. Scalone, M. Beller, Synthesis of nickel nanoparticles with N-Doped graphene shells for catalytic reduction reactions, ChemCatChem 8 (2016) 129–134.
[36] X. Sun, A.I. Olivos-Suarez, L. Oar-Arteta, E. Rozhko, D. Osadchii, A. Bavykina, F. Kapteijn, J. Gascon, Metal-organic framework mediated cobalt/nitrogen-doped carbon hybrids as efficient and chemoselective catalysts for the hydrogenation of nitroarenes, ChemCatChem 9 (2017) 1854–1862.
[37] W.-J. Liu, K. Tian, H. Jiang, One-pot synthesis of Ni-NiFe2O4/carbon nanofiber composites from biomass for selective hydrogenation of aromatic nitro compounds, Green Chem. 17 (2015) 821–826.
[38] L. Liu, P. Concepción, A. Corma, Non-noble metal catalysts for hydrogenation: a facile method for preparing Co nanoparticles covered with thin layered carbon, J. Catal. 340 (2016) 1–9.
[39] L. Liu, F. Gao, P. Concepción, A. Corma, A new strategy to transform mono and bimetallic non-noble metal nanoparticles into highly active and chemoselective hydrogenation catalysts, J. Catal. 350 (2017) 218–225.
[40] F. Zhang, C. Zhao, S. Chen, H. Li, H. Yang, X.-M. Zhang, In situ mosaic strategy generated Co-based N-doped mesoporous carbon for highly selective hydrogenation of nitroaromatics, J. Catal. 348 (2017) 212–222.

[41] X. Wang, Y. Li, Chemoselective hydrogenation of functionalized nitroarenes using MOF-derived co-based catalysts, J. Mol. Catal. A: Chem. 420 (2016) 56–65.
[42] F.A. Westerhaus, R.V. Jagadeesh, G. Wienhöfer, M.-M. Pohl, J. Radnik, A.-E. Surkus, J. Rabeah, K. Junge, H. Junge, M. Nielsen, A. Brückner, M. Beller, Heterogenized cobalt oxide catalysts for nitroarene reduction by pyrolysis of molecularly defined complexes, Nat. Chem. 5 (2013) 537–543.
[43] R.V. Jagadeesh, D. Banerjee, P.B. Arockiam, H. Junge, K. Junge, M.-M. Pohl, J. Radnik, A. Bruckner, M. Beller, Highly selective transfer hydrogenation of functionalised nitroarenes using cobalt-based nanocatalysts, Green Chem. 17 (2015) 898–902.
[44] D. Formenti, C. Topf, K. Junge, F. Ragaini, M. Beller, Fe2O3/NGr@C- and Co-Co3O4/NGr@C-catalysed hydrogenation of nitroarenes under mild conditions, Catal. Sci. Technol. 6 (2016) 4473–4477.
[45] K. Shen, L. Chen, J. Long, W. Zhong, Y. Li, MOFs-templated Co@Pd core-shell NPs embedded in n-doped carbon matrix with superior hydrogenation activities, ACS Catal. 5 (2015) 5264–5271.
[46] P. Zhou, L. Jiang, F. Wang, K. Deng, K. Lv, Z. Zhang, High performance of a cobalt–nitrogen complex for the reduction and reductive coupling of nitro compounds into amines and their derivatives, Sci. Adv. 3 (2017).
[47] X.-C. Huang, Y.-Y. Lin, J.-P. Zhang, X.-M. Chen, Ligand-directed strategy for zeolite-type metal-organic frameworks: zinc(II) imidazolates with unusual zeolitic topologies, Angew. Chem. Int. Ed. 45 (2006) 1557–1559.
[48] K.S. Park, Z. Ni, A.P. Côté, J.Y. Choi, R. Huang, F.J. Uribe-Romo, H.K. Chae, M. O'Keeffe, O.M. Yaghi, Exceptional chemical and thermal stability of zeolitic imidazolate frameworks, Proc. Natl. Acad. Sci. 103 (2006) 10186–10191.
[49] R. Banerjee, A. Phan, B. Wang, C. Knobler, H. Furukawa, M. O'Keeffe, O.M. Yaghi, High-throughput synthesis of zeolitic imidazolate frameworks and application to CO2 capture, Science 319 (2008) 939–943.
[50] J. Tang, R.R. Salunkhe, J. Liu, N.L. Torad, M. Imura, S. Furukawa, Y. Yamauchi, Thermal conversion of core-shell metal–organic frameworks: a new method for selectively functionalized nanoporous hybrid carbon, J. Am. Chem. Soc. 137 (2015) 1572–1580.
[51] J. Yang, F. Zhang, H. Lu, X. Hong, H. Jiang, Y. Wu, Y. Li, Hollow Zn/Co ZIF particles derived from core-shell ZIF-67@ZIF-8 as selective catalyst for the semi-hydrogenation of acetylene, Angew. Chem. Int. Ed. 54 (2015) 10889–10893.
[52] Y.-Z. Chen, C. Wang, Z.-Y. Wu, Y. Xiong, Q. Xu, S.-H. Yu, H.-L. Jiang, From bimetallic metal-organic framework to porous carbon: high surface area and multicomponent active dopants for excellent electrocatalysis, Adv. Mater. 27 (2015) 5010–5016.
[53] P. Yin, T. Yao, Y. Wu, L. Zheng, Y. Lin, W. Liu, H. Ju, J. Zhu, X. Hong, Z. Deng, G. Zhou, S. Wei, Y. Li, Single cobalt atoms with precise N-coordination as superior oxygen reduction reaction catalysts, Angew. Chem. Int. Ed. 55 (2016) 10800–10805.
[54] J. Tang, R.R. Salunkhe, H. Zhang, V. Malgras, T. Ahamad, S.M. Alshehri, N. Kobayashi, S. Tominaka, Y. Ide, J.H. Kim, Y. Yamauchi, Bimetallic metal-organic frameworks for controlled catalytic graphitization of nanoporous carbons, Sci. Rep. 6 (2016) 30295.
[55] X. Kang, H. Liu, M. Hou, X. Sun, H. Han, T. Jiang, Z. Zhang, B. Han, Synthesis of supported ultrafine non-noble subnanometer-scale metal particles derived from metal-organic frameworks as highly efficient heterogeneous catalysts, Angew. Chem. 128 (2016) 1092–1096.
[56] H. Li, H. Yang, H. Li, Highly active mesoporous Co–B amorphous alloy catalyst for cinnamaldehyde hydrogenation to cinnamyl alcohol, J. Catal. 251 (2007) 233–238.
[57] M.F. De Lange, T.J.H. Vlugt, J. Gascon, F. Kapteijn, Adsorptive characterization of porous solids: error analysis guides the way, Micropor. Mesopor. Mater. 200 (2014) 199–215.
[58] L.A. Grunes, Study of the K edges of 3d transition metals in pure and oxide form by x-ray-absorption spectroscopy, Phys. Rev. B 27 (1983) 2111–2131.
[59] B. Ravel, M. Newville, ATHENA, ARTEMIS, HEPHAESTUS: data analysis for X-ray absorption spectroscopy using IFEFFIT, J. Synchrotron Radiat. 12 (2005) 537–541.
[60] B. Ravel, M. Newville, ATHENA, ARTEMIS, HEPHAESTUS: data analysis for X-ray absorption spectroscopy using IFEFFIT, J. Synchrotron Radiat. 12 (2005) 537–541.
[61] H. Fei, J. Dong, M.J. Arellano-Jiménez, G. Ye, N. Dong Kim, E.L.G. Samuel, Z. Peng, Z. Zhu, F. Qin, J. Bao, M.J. Yacaman, P.M. Ajayan, D. Chen, J.M. Tour, Atomic cobalt on nitrogen-doped graphene for hydrogen generation, Nat. Commun. 6 (2015) 8668.
[62] B.Y. Xia, Y. Yan, N. Li, H.B. Wu, X.W. Lou, X. Wang, A metal–organic framework-derived bifunctional oxygen electrocatalyst, Nat. Energy 1 (2016) 15006.
[63] P. Zhou, Z. Zhang, One-pot reductive amination of carbonyl compounds with nitro compounds by transfer hydrogenation over Co–Nx as catalyst, ChemSusChem 10 (2017) 1892–1897.
[64] Q. Wang, X. Qiu, W. Hu, Y. Huang, Facile synthesis of three-dimensional porous nitrogen doped carbon supported Co3O4 for oxygen reduction reaction and oxygen evolution reaction, Mater. Lett. 190 (2017) 169–172.
[65] P. Zhou, Z. Zhang, L. Jiang, C. Yu, K. Lv, J. Sun, S. Wang, A versatile cobalt catalyst for the reductive amination of carbonyl compounds with nitro compounds by transfer hydrogenation, Appl. Catal. B 210 (2017) 522–532.
[66] J.R. Pels, F. Kapteijn, J.A. Moulijn, Q. Zhu, K.M. Thomas, Evolution of nitrogen functionalities in carbonaceous materials during pyrolysis, Carbon 33 (1995) 1641–1653.
[67] J. Casanovas, J.M. Ricart, J. Rubio, F. Illas, J.M. Jiménez-Mateos, Origin of the large N 1s binding energy in X-ray photoelectron spectra of calcined carbonaceous materials, J. Am. Chem. Soc. 118 (1996) 8071–8076.
[68] L. Shang, H. Yu, X. Huang, T. Bian, R. Shi, Y. Zhao, G.I.N. Waterhouse, L.-Z. Wu, C.-H. Tung, T. Zhang, Well-dispersed ZIF-derived Co, N-Co-doped carbon nanoframes through mesoporous-silica-protected calcination as efficient oxygen reduction electrocatalysts, Adv. Mater. 28 (2016) 1668–1674.
[69] F. Hillman, J.M. Zimmerman, S.-M. Paek, M.R.A. Hamid, W.T. Lim, H.-K. Jeong, Rapid microwave-assisted synthesis of hybrid zeolitic-imidazolate frameworks with mixed metals and mixed linkers, J. Mater. Chem. A 5 (2017) 6090–6099.
[70] H. Wang, C.Y. Ralston, D.S. Patil, R.M. Jones, W. Gu, M. Verhagen, M. Adams, P. Ge, C. Riordan, C.A. Marganian, P. Mascharak, J. Kovacs, C.G. Miller, T.J. Collins, S. Brooker, P.D. Croucher, K. Wang, E.I. Stiefel, S.P. Cramer, Nickel L-Edge Soft X-ray spectroscopy of nickel−iron hydrogenases and model compoundsevidence for high-spin nickel(II) in the active enzyme, J. Am. Chem. Soc. 122 (2000) 10544–10552.
[71] A. Sharma, M. Varshney, H.J. Shin, B.-H. Lee, K.H. Chae, S.O. Won, Effect of Cu insertion on structural, local electronic/atomic structure and photocatalyst properties of TiO2, ZnO and Ni(OH)2 nanostructures: XANES-EXAFS study, Mater. Chem. Phys. 191 (2017) 129–144.
[72] G. Frank de, V. György, G. Pieter, The 1s x-ray absorption pre-edge structures in transition metal oxides, J. Phys.: Condens. Matter, 21 (2009) 104207.
[73] N.L. Torad, M. Hu, S. Ishihara, H. Sukegawa, A.A. Belik, M. Imura, K. Ariga, Y. Sakka, Y. Yamauchi, Direct synthesis of MOF-derived nanoporous carbon with magnetic Co nanoparticles toward efficient water treatment, Small 10 (2014) 2096–2107.
[74] B. Liu, H. Shioyama, T. Akita, Q. Xu, Metal-organic framework as a template for porous carbon synthesis, J. Am. Chem. Soc. 130 (2008) 5390–5391.
[75] Y.J. Sa, D.-J. Seo, J. Woo, J.T. Lim, J.Y. Cheon, S.Y. Yang, J.M. Lee, D. Kang, T.J. Shin, H.S. Shin, H.Y. Jeong, C.S. Kim, M.G. Kim, T.-Y. Kim, S.H. Joo, A general approach to preferential formation of active Fe–Nx sites in Fe–N/C electrocatalysts for efficient oxygen reduction reaction, J. Am. Chem. Soc. 138 (2016) 15046–15056.